Research Article | Vol. 29, No. 8 / 12 April 2021 / Optics Express 11635
Optics EXPRESS

Role of electric currents in the Fano resonances of connected plasmonic structures

MARCO RICCARDI AND OLIVIER J. F. MARTIN*

Nanophotonics and Metrology Laboratory, Swiss Federal Institute of Technology Lausanne (EPFL), EPFL-STI-NAM, Station 11, CH- 1015 Lausanne, Switzerland
*olivier.martin@epfl.ch

Abstract: In this work, we use finite elements simulations to study the far field properties of two plasmonic structures, namely a dipole antenna and a cylinder dimer, connected to a pair of nanorods. We show that electrical, rather than near field, coupling between the modes of these structures results in a characteristic Fano lineshape in the far field spectra. This insight provides a way of tailoring the far field properties of such systems to fit specific applications, especially maintaining the optical properties of plasmonic antennas once they are connected to nanoelectrodes. This work extends the previous understanding of Fano resonances as generated by a simple near field coupling and provides a route to an efficient design of functional plasmonic electrodes.

1. Introduction

The design and fabrication of increasingly complex plasmonic structures is quickly becoming a key requirement to advance fields such as plasmonic and nanophotonic circuits [1–5], metamaterials [6–8] and sensing [1,7–9]. In particular, plasmonic electrodes are finding a growing number of applications thanks to their ability to simultaneously control electrical and optical signals, and their capabilities have already been demonstrated in a number of works in a variety of fields, ranging from optoelectronics [10–12] to biosensing [13–15] and hot electrons chemistry [5,16], to name a few. In these systems, comprised of multiple plasmonic structures, Fano resonances can arise from the coupling between two spectrally-overlapping modes and can greatly affect the near and far field properties of the device [17–21]. These resonances have been intensively studied during the past decade and indeed Fano-resonant systems have found applications in many different fields such as biosensing [7,22,23], optical switching [24–27] and chirality [28–30]. Achieving full control over the Fano response of such structures could provide additional degrees of freedom to these systems, making them potentially more versatile and expanding their range of applications. Traditionally, mechanical or electrical techniques have been used to tune the strength of Fano resonances [31–33], while the role of the mode coupling has been mainly overlooked. This coupling can occur through either field or current interactions. In the former, capacitive near field coupling in a nanogap can promote mode coupling and hybridization; this has been extensively studied in the literature [22,23,34]. In addition, retardation effects can be introduced which allow the excitation of both electric and magnetic modes, whose interference will result in a so-called magnetic Fano resonance [35–37]. The role of current coupling on the other hand, even though it has enjoyed some attention from the plasmonic community [38–40], has been mainly overlooked in the Fano resonances literature, with a few notable exceptions [29,41,42]. In these works, the authors exploited arrays of metallic nanoapertures with 3D structures to generate Fano resonances arising from the coupling between the bright extraordinary optical transmission mode of the lattice and the dark localized surface plasmon resonance modes of the 3D structure. They further identified the current as the dominant coupling mechanism in this system, providing the first demonstration of current (resistive) coupling in Fano-resonant structures. Here on the other hand, we present the first demonstration of such a coupling mechanism in planar plasmonic

#421951 https://doi.org/10.1364/OE.421951
Journal © 2021 Received 5 Feb 2021; revised 18 Mar 2021; accepted 22 Mar 2021; published 30 Mar 2021

Optics EXPRESS

structures, more suited for applications in plasmonic circuitry, and provide a way of geometrically tuning the Fano response of these systems for their specific application.

2. Results and discussion

We start by studying the electrically connected antenna structure proposed in [43] and shown in Fig. 1, on the left. It is composed of a plasmonic dipole antenna connected to two nanorods which act as nanoelectrodes, feeding the antenna and allowing it to function as an emitter and receiver of optical radiation [12,44]. Similar dimer systems have also been employed for sensing or signal processing applications and are therefore of great interest [45,46]. Figure 2(a) shows the simulated far field spectra of the isolated components of this structure (i.e. the antenna and the electrodes), which clearly show both the antenna's and electrodes' dipolar resonances at 815 nm and 580 nm respectively. Here and throughout this work, 3D simulations were performed with a commercial FEM software (COMSOL Multiphysics 5.3) by evaluating the far field norm on a sphere surrounding the structures. These were made of gold [47] in a water environment (n=1.33) and were excited with an x-polarised plane wave travelling along the z axis. We neglected the presence of a substrate below the structures, whose main effect would only be, for conventional dielectric substrates, to spectrally redshift the resonances of the system. Metallic or high-dielectric constant substrates might on the other hand play a more active role in the generation of Fano resonances [48,49]. Similar results were obtained with a custom-made software based on the surface integral equation approach [50]. From the experimental side, such structures can be fabricated using top-down cleanroom techniques such as electron beam lithography or focused ion beam milling [43,51,52]. Figure 2(b) shows the spectra of the connected structure for electrodes placed 55 nm (blue plot) and 70 nm (red line) away from the center of the gap. One can clearly see that, while for δ = 55 nm the overall spectrum is just the superposition of the two spectra in Fig. 2(a), for δ = 70 nm two asymmetric dips appear in the far field profile. We can relate these dips to Fano resonances which originate from the coupling between the antenna's dipolar bright mode [i.e. the black plot in Fig. 2(a)] and high-order dark modes in the electrodes, which are shown in green in Fig. 2(b) and appear as a result of Fabry-Perot types of resonances, as shown in Fig. S1, roughly at the same wavelengths as the dips. Moreover, one can note that, as the electrodes are made longer and can therefore support more high-order modes, more dips appear in the far field spectrum (not shown here), thus corroborating this interpretation. As the rods length reaches the onset for the excitation of propagating modes [53], the excited dipolar mode in the antenna can couple to the dark SPP leading to a significant broadening of the resonance, as it has been already shown in [43]. Here, we quantify the amplitude of the Fano resonance by the difference between the far field value at the bottom of the Fano dip [red line in Fig. 2(b)] and its value, at the same wavelength, in the case where no Fano resonance is present [blue line in Fig. 2(b)]. This amplitude is indicated with a black line in Fig. 2(b). This simple approach agrees well with the computation of the modulation damping, defined as the fraction of the total light intensity that does not contribute to the interference in the far field [54,55]. For the case of δ = 55 nm the modulation damping yields a value of 1, while it quickly decreases and approaches 0 for other values of δ.

Figure S2 in the supporting information provides additional spectra for other values of δ and shows how, by inserting the electrodes at different positions in the antenna, the strength of the Fano resonance can be arbitrarily tuned and even brought to zero for δ = 55 nm. Clearly, the position of the nanorods with respect to the antenna affects the coupling strength between the modes of both structures. In order to minimize this coupling and preserve the far field properties of the antenna, it was proposed to connect the electrodes at the position where the near field of the isolated antenna takes its minimum value [43]. In this way, one would reduce the near field coupling between the two structures and retain a clean far field spectra free of Fano resonances. To this end, Fig. 3 shows, in red, a plot of the electric near field of the isolated dipole nanoantenna.

Optics EXPRESS

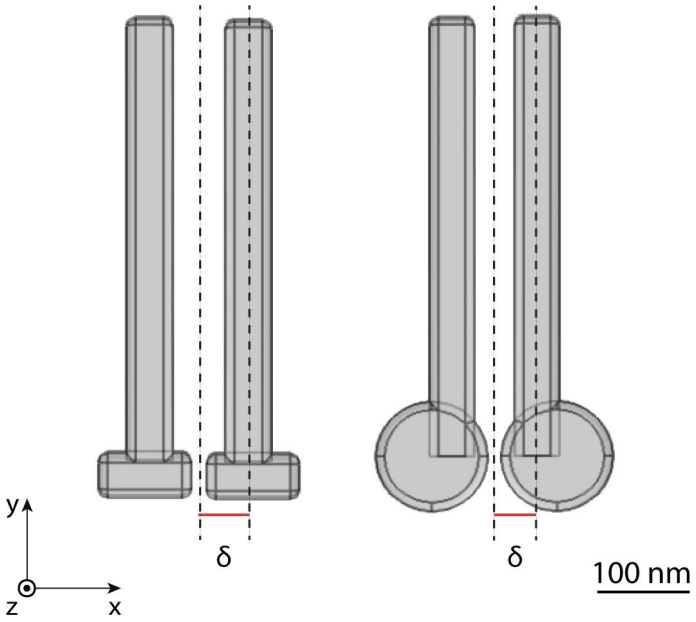

Fig. 1. Schematic of the studied geometries. The antenna, on the left, is 220 nm long, 50 nm wide and 40 nm thick, with a 20 nm gap between the two arms. The cylinders, on the right, have a diameter of 125 nm and are 40 nm thick, with a 20 nm gap between them. The electrodes are, in both cases, 500 nm long, 50 nm wide and 40 nm thick and are placed at different distances δ, indicated by the red line, from the center of the gap. The structures are symmetric in the z=0 plane.

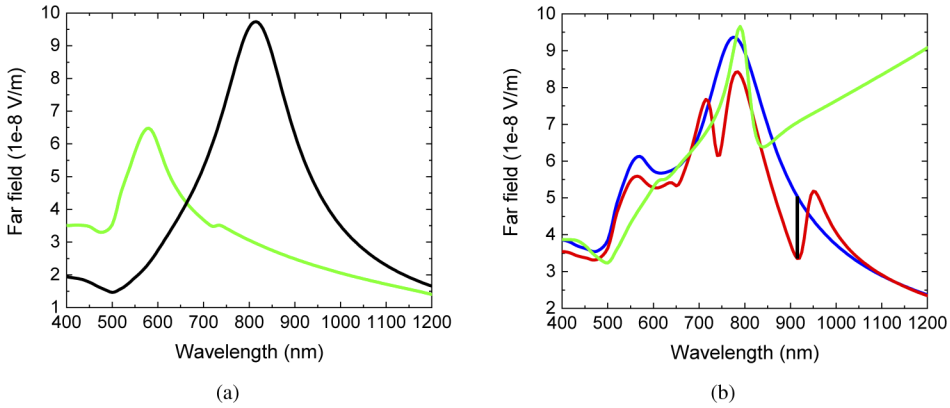

Fig. 2. (a) Far field norm for the isolated electrodes (δ = 55 nm, green) and antenna (black) for x-polarised excitation. (b) Far field norm of the connected antenna for δ = 55 nm (blue) and δ = 70 nm (red) under x-polarised excitation. In green, the far field norm of the isolated electrodes (δ = 70 nm) for y-polarised excitation, showing the dark modes of the electrodes. The black vertical line shows the empirical amplitude of the Fano resonance.

Optics EXPRESS

It also shows in blue, for different positions of the nanorods, the amplitude of the Fano resonance appearing in the far field spectrum of the connected structure around λ = 920 nm. Fig. 3 clearly shows how the Fano amplitude correlates well with the near field distribution, with the resonance disappearing from the far field spectrum when the electrodes are connected to the antenna at the point of weakest near field, thus corroborating this near field coupling model. A similar analysis, with the same conclusions, can be carried out for the other Fano resonance around λ = 750 nm, Fig. 2(b).

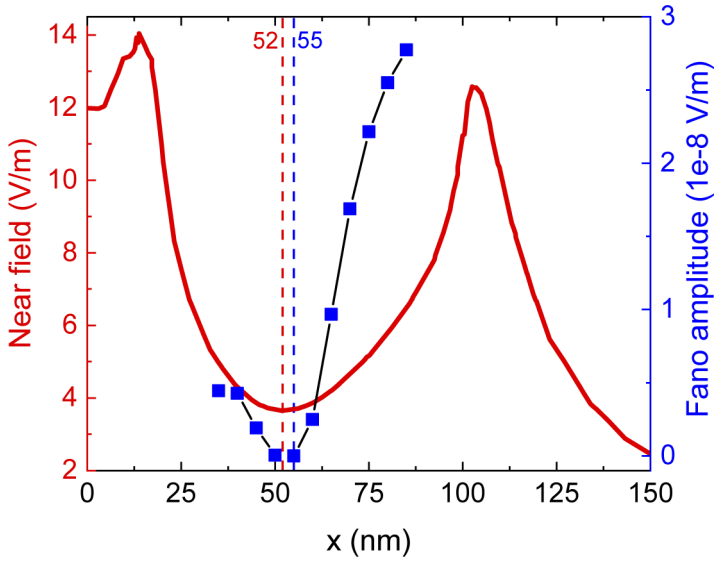

Fig. 3. Antenna's near field amplitude (red line) and Fano resonance magnitude (blue squares) for different electrodes positions. The two vertical dashed lines show the minimum of the field and of the Fano amplitude. The field is evaluated along a line at z=0 lying 0.5 nm away from the structure and the origin of the x axis is placed in the center of the gap, as indicated in Fig. 1.

It is interesting to extend this concept to different structures, which may provide an easier fabrication or offer different optical properties that could suit better a specific application. We therefore move our analysis to a different system, depicted in Fig. 1 on the right, composed of a cylinder dimer connected to a pair of nanorods, which again can play the role of nanoelectrodes. Figure 4(a) shows the far field profile of such a structure for two different electrodes positions and, here again, we see that this position can regulate the appearance and strength of Fano resonances in the far field. However, as Fig. 4(b) clearly shows, the near field interactions do not seem to control the amplitude of this resonance anymore, as we still retain a small Fano resonance even when the electrodes are connected at the position of field minimum at 55 nm [see the red plot in Fig. 4(a)]. The near field coupling model therefore fails to describe the properties of this structure, which needs further investigations to elucidate the coupling mechanisms at play. To this end, Fig. 5 shows the far field norm, the electric near field and the current flowing in the structure, at the Fano resonance wavelength, for different δ. Here one can see that, as the electrodes are moved from one end to the other of the cylinders, the far field abruptly changes, with different Fano resonances appearing with varying strengths [Fig. 5(a)]. For the very specific case of δ = 65 nm, these resonances are completely cancelled and one obtains a clean far field profile. If we now have a look at the field distribution [Fig. 5(b)], we can see that the only field enhancement occurring in these structures is the one between the two electrodes or the two disks, which doesn't produce any Fano feature and is not analyzed here. One can further note that the

Optics EXPRESS

usual strong near field enhancement typical of Fano resonances, occurring in the gap between the interacting structures and signature of strong near field coupling [18], is not present between the electrodes and the disks. Indeed, as the electrodes and the cylinders are in contact with one another, there is no gap between them and no capacitive near field coupling can therefore occur. On the other hand, by looking at the current distribution inside the structure [Fig. 5(c), on top] one can notice how, when Fano resonances are present in the far field spectrum, there is a current flowing inside the electrodes which can excite the high order dark modes responsible for the appearance of the Fano feature. Surprisingly, for $\delta = 65$ nm, no current flows into the rods and, consequently, no Fano resonance appears in the far field. If we zoom in to the electrodes/cylinders boundary and additionally plot the direction of the current flow (Fig. 5(c), on the bottom), we can see that when a net current leaks from the disks to the nanorods, dark modes can be electrically excited in the electrodes in just the same way as a near field interaction would. Figure S4 in the supporting information gives further insights about the strength of the bright mode for different positions of the electrodes.

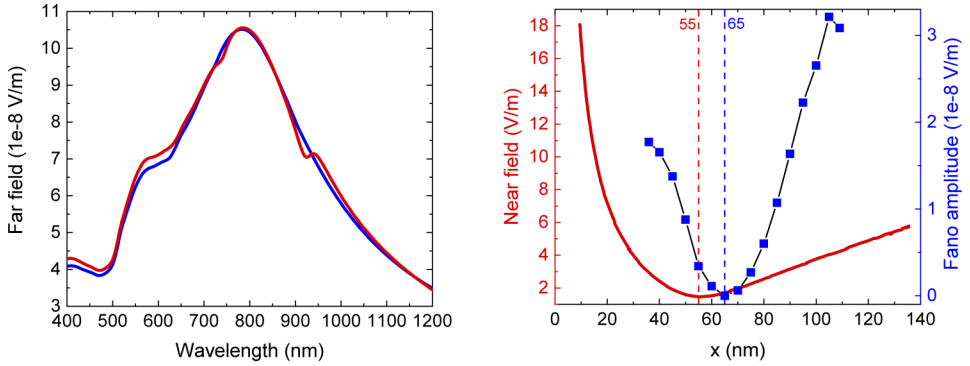

Fig. 4. (a) Far field norm of the connected cylinders for $\delta = 65$ nm (blue) and 55 nm (red) for x-polarized excitation. Additional spectra are shown in Fig. S3 in the supporting information. (b) Plot of the cylinders near field and of the amplitude of the Fano resonance for different positions of the nanorods. The two vertical dashed lines show the minimum of the field and of the Fano amplitude. As before, this amplitude refers to the second resonance appearing at longer wavelengths in (a), while the field is evaluated along a line at z=0 laying 0.5 nm away from the structure and the origin of the x axis is always placed in the center of the gap.

The coupling mechanism seems therefore to be the following: as the bright dipolar mode in the cylinders is excited by the impinging light, electrons oscillations are induced in the structure which result in the generation of an electrical current. This current, under proper conditions, can leak to the electrodes and excite dark modes. These will then be able to interfere with the bright mode by imprinting their characteristic Fano signature in the far field spectrum. In this context, the case of $\delta = 65$ nm is very interesting because, at this position, the current leakage is minimized leading to vanishing coupling between the cylinders and the electrodes. This is even more surprising if one recalls that the total current distribution J in a resonant structure takes its maximum value around the center of the geometry, where the field is minimum, and quickly goes to zero towards the ends of the structure [56]. Consequently, one would expect to have a stronger coupling (i.e. stronger Fano resonances) when the rods are connected near the center of the cylinders where the current is strong and weaker coupling for end-connected structures, in contrast to what is reported here. However, as the interaction between the rods and the cylinders takes place on their touching boundaries, we are more interested in studying the

Optics EXPRESS

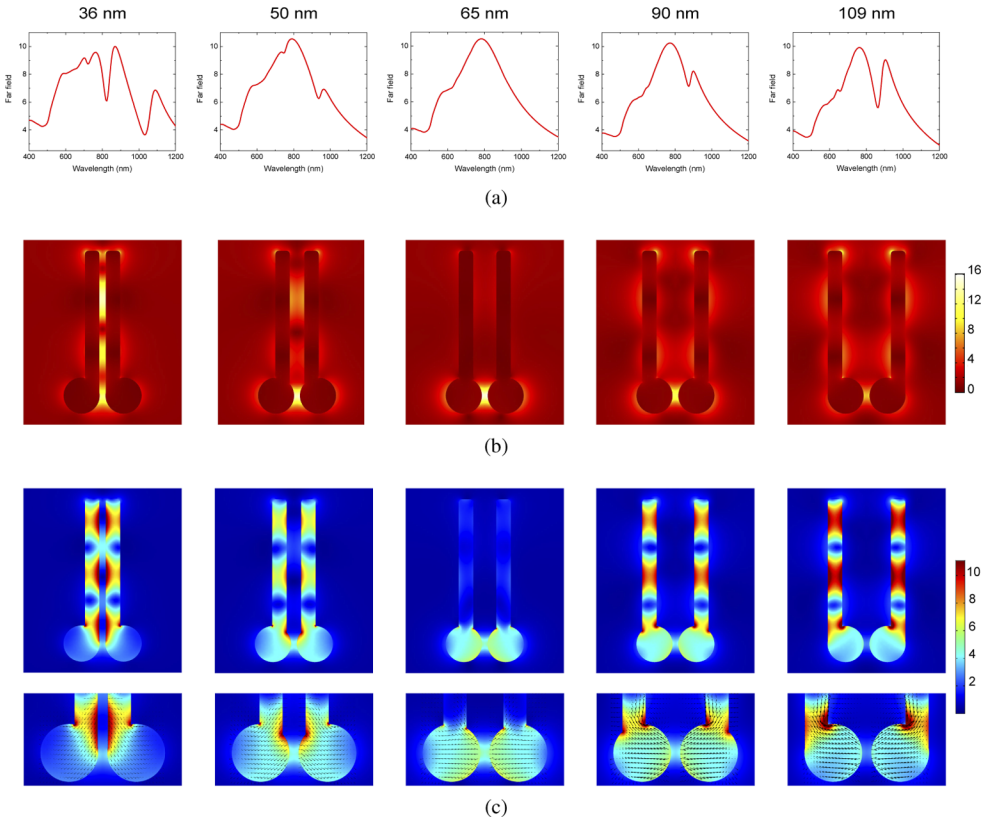

Fig. 5. (a) Far field norm and (b) relative electric field amplitude and (c) current density maps shown at the wavelength of the Fano resonance, ~ 920 nm, for the connected cylinders for different values of δ (shown on top). The far and near field units are $10^{-8}V/m$ and V/m, while the current density is expressed in $10^{5}A/m^{2}$. See Visualization 1 for additional data for different δ.

current distribution on the surface of these structures. We can see in Fig. S5 in the supporting document that, contrary to what happens in the bulk, the current density on the surface roughly follows the field profile and reaches a minimum around the center of the structure. We can further note that the current leakage from the cylinders to the electrodes is proportional only to the vertical J_y component of the current, which follows a similar behaviour and reaches its minimum at 59 nm, thus corroborating this current coupling model.

To further investigate resistive coupling in our system, we used a series of two coupled RLC circuits to simulate the frequency response of this geometry. Resonant circuits have already been used to model the Fano properties of plasmonic structures using either capacitors [57,58] or inductors [59,60] to study the near field coupling between different plasmonic elements. However, the resistive coupling between the bright dipolar mode in the disks and the dark modes in the electrodes in our system is better modeled with a resistance R whose value can tune the coupling strength between the two branches of the circuit, as shown in Fig. 6(a). Here, the left branch is driven by a sinusoidal AC voltage and represents therefore the bright dipolar mode which is directly excited by the impinging light. The right branch on the other hand, represents the dark mode in the nanorod and can only be excited through current leakage from the left branch, which is controlled by the coupling resistance R. The lager R, the more current will flow into the dark mode and the stronger the coupling will be. However, for small values of R the current

Optics EXPRESS

will preferably pass through the coupling resistance than through the second RLC circuit, which will therefore be very weakly excited and will not strongly affect the frequency response of the total system, as shown in Fig. 6(b). We can see here that, for vanishing coupling (R = 0 Ω), the Fano resonance completely disappears from the frequency spectrum, mimicking the case of perfectly-connected structures shown in blue in Fig. 2(b) and Fig. 4(a). As the value of R increases, the coupling becomes stronger and so does the Fano resonance, until we reach the point (R = 5 TΩ) where no current can flow anymore through R and the resonance completely disappears (this case does not have an optical analogue). More details about this electrical circuit modelling are provided in the Supplemental Document 1, particularly in Fig. S6.

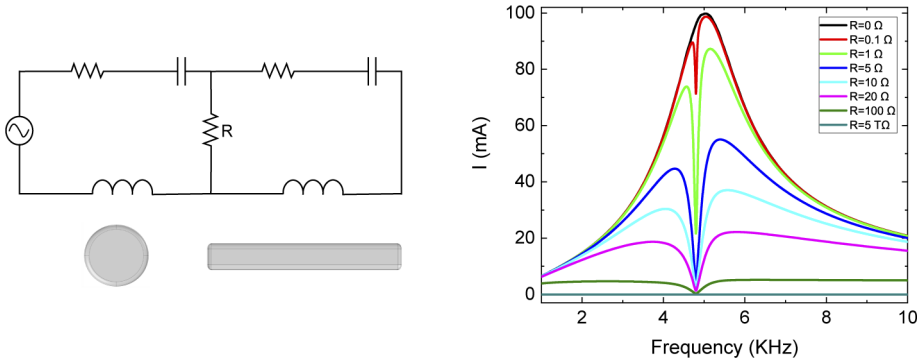

Fig. 6. (a) The two coupled RLC circuits used to model the bright and dark plasmonic modes of our system. The bright mode in the cylinders is represented by the left branch, which is excited with a sinusoidal 1 V peak voltage, while the right branch represents the dark mode in the nanorods. (b) Plot of the current flowing through the coupling resistance R for different values of the latter.

After identifying the electrical current, and in particular J_y, as the main promoter of mode coupling in these connected plasmonic structures, it is now trivial to find the position of the connecting nanorods in order not to affect the far field resonance of the isolated structure: this position will be the one where J_y goes to zero, i.e. where the coupling is minimized. To this end, Fig. 7(a) shows the J_y profile on the cylinders' surface together with the Fano amplitude for different positions of the electrodes and demonstrates indeed a better agreement between the two curves than in Fig. 4(b). Moreover, Fig. 7(b) also shows how this current coupling model can be used to explain the behaviour of the connected antenna, as its Fano resonance also disappears approximately where J_y vanishes. We can therefore see how resistive coupling can account for the response of both the antenna and the cylinders, while the near field coupling model cannot properly describe the behaviour of the cylinders. We speculate here that in these round structures the current distribution follows a more complex pattern, in such a way that the zero of J_y doesn't necessarily correspond to the zero of the near field, leading to a clear failure of the capacitive near field coupling model.

Optics EXPRESS

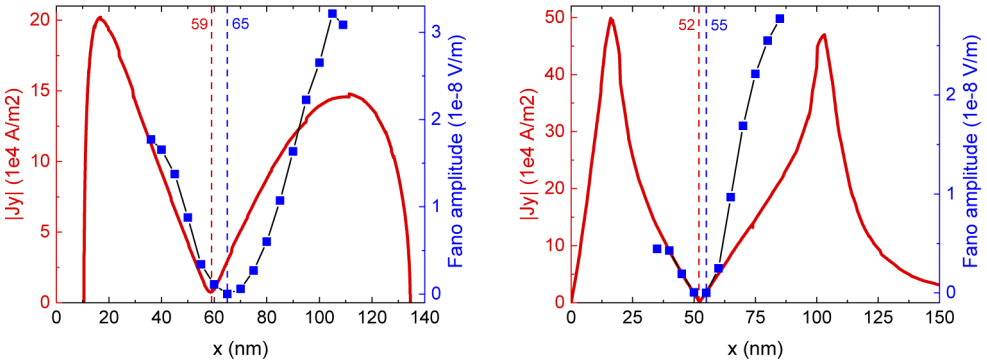

Fig. 7. (a) Plot of |Jy| on the lateral surface of the cylinders and of the amplitude of the second Fano resonance for different positions of the electrodes. The two vertical dashed lines indicate the minimum of the field and of the Fano amplitude. (b) Same plot as in (a), but for the connected antenna.

3. Conclusions

In this work we provided a theoretical framework to explain the rich optical spectra of compound plasmonic structures arising from the coupling between different modes of the system. We studied the near-field and electrical current interactions between different parts of the structure and identified the latter as the main contributor to the coupling, providing a way to tailor the far field properties of such systems to fit specific applications. In particular, we demonstrated the possibility of connecting nanoscale electrodes to plasmonic structures without affecting their far field optical response. This work extends the previous understanding of the Fano coupling mechanism in planar plasmonic structures by showing how the near field coupling model, even though it doesn't always capture the full essence of the coupling mechanism, can still be used in the design of compound "straight" plasmonic structures, but fails when round structures come into play. By identifying the current as the main coupling mechanism, the model proposed here allows the design of more complex and versatile structures, which are likely to play a major role in emerging optical and quantum technologies.

Funding. European Research Council (ERC-2015-AdG-695206 Nanofactory).

Disclosures. The authors declare no conflicts of interest.

Supplemental document. See Supplement 1 for supporting content.

References

1. M. Alavirad, S. Siadat Mousavi, L. Roy, and P. Berini, "Schottky-contact plasmonic dipole rectenna concept for biosensing," Opt. Express **21**(4), 4328–4347 (2013).
2. M. N. Gadalla, M. Abdel-Rahman, and A. Shamim, "Design, Optimization and Fabrication of a 28.3 THz Nano-Rectenna for Infrared Detection and Rectification," Sci. Rep. **4**(1), 4270 (2015).
3. P. Vavassori, M. Pancaldi, M. J. Perez-Roldan, A. Chuvilin, and A. Berger, "Remote Magnetomechanical Nanoactuation," Small **12**(8), 1013–1023 (2016).
4. Z.-J. Yang, T. J. Antosiewicz, and T. Shegai, "Role of material loss and mode volume of plasmonic nanocavities for strong plasmon-exciton interactions," Opt. Express **24**(18), 20373–20381 (2016).
5. R. M. Osgood III, M. Kang, K.-B. Kim, Y. Ait-El-Aoud, S. Dinneen, S. Kooi, G. Fernandes, and J. M. Xu, "Nanorectenna spectrally-selective plasmonic hot electron response to visible-light lasers," Nanotechnology **31**(13), 135207 (2020).
6. F. Monticone and A. Alù, "Metamaterial, plasmonic and nanophotonic devices," Rep. Prog. Phys. **80**(3), 036401 (2017).
7. C. Wu, A. B. Khanikaev, R. Adato, N. Arju, A. A. Yanik, H. Altug, and G. Shvets, "Fano-resonant asymmetric metamaterials for ultrasensitive spectroscopy and identification of molecular monolayers," Nat. Mater. **11**(1), 69–75 (2012).

Optics EXPRESS

8. R. Verre, N. Maccaferri, K. Fleischer, M. Svedendahl, N. O. Länk, A. Dmitriev, P. Vavassori, I. V. Shvets, and M. Käll, "Polarization conversion-based molecular sensing using anisotropic plasmonic metasurfaces," Nanoscale **8**(20), 10576–10581 (2016).
9. N. Tolga Yardimci and M. Jarrahi, "High Sensitivity Terahertz Detection through Large-Area Plasmonic Nano-Antenna Arrays," Sci. Rep. **7**(1), 42667 (2017).
10. C. W. Berry, N. Wang, M. R. Hashemi, M. Unlu, and M. Jarrahi, "Significant performance enhancement in photoconductive terahertz optoelectronics by incorporating plasmonic contact electrodes," Nat. Commun. **4**(1), 1622 (2013).
11. R. Bartholomew, C. Williams, A. Khan, R. Bowman, and T. Wilkinson, "Plasmonic nanohole electrodes for active color tunable liquid crystal transmissive pixels," Opt. Lett. **42**(14), 2810 (2017).
12. R. Kullock, M. Ochs, P. Grimm, M. Emmerling, and B. Hecht, "Electrically-driven Yagi-Uda antennas for light," Nat. Commun. **11**(1), 115 (2020).
13. A. Barik, L. M. Otto, D. Yoo, J. Jose, T. W. Johnson, and S. H. Oh, "Dielectrophoresis-enhanced plasmonic sensing with gold nanohole arrays," Nano Lett. **14**(4), 2006–2012 (2014).
14. C. Schäfer, D. P. Kern, and M. Fleischer, "Capturing molecules with plasmonic nanotips in microfluidic channels by dielectrophoresis," Lab Chip **15**(4), 1066–1071 (2015).
15. M. Dipalo, G. C. Messina, H. Amin, R. La Rocca, V. Shalabaeva, A. Simi, A. Maccione, P. Zilio, L. Berdondini, and F. De Angelis, "3D plasmonic nanoantennas integrated with MEA biosensors," Nanoscale **7**(8), 3703–3711 (2015).
16. P. Zilio, M. Dipalo, F. Tantussi, G. C. Messina, and F. de Angelis, "Hot electrons in water: injection and ponderomotive acceleration by means of plasmonic nanoelectrodes," Light: Sci. Appl. **6**(6), e17002 (2017).
17. B. Luk'yanchuk, N. I. Zheludev, S. A. Maier, N. J. Halas, P. Nordlander, H. Giessen, and C. Tow Chong, "The Fano resonance in plasmonic nanostructures and metamaterials," Nat. Mater. **9**(9), 707–715 (2010).
18. B. Gallinet and O. J. F. Martin, "Relation between near–field and far–field properties of plasmonic Fano resonances," Opt. Express **19**(22), 22167–22175 (2011).
19. B. Gallinet and O. J. F. Martin, "Influence of Electromagnetic Interactions on the Line Shape of Plasmonic Fano Resonances," ACS Nano **5**(11), 8999–9008 (2011).
20. B. Gallinet and O. J. F. Martin, "Refractive Index Sensing with Subradiant Modes: A Framework To Reduce Losses in Plasmonic Nanostructures," ACS Nano **7**(8), 6978–6987 (2013).
21. M. F. Limonov, M. V. Rybin, A. N. Poddubny, and Y. S. Kivshar, "Fano resonances in photonics," Nat. Photonics **11**(9), 543–554 (2017).
22. J. B. Lassiter, H. Sobhani, J. A. Fan, J. Kundu, F. Capasso, P. Nordlander, and N. J. Halas, "Fano Resonances in Plasmonic Nanoclusters: Geometrical and Chemical Tunability," Nano Lett. **10**(8), 3184–3189 (2010).
23. A. Dutta, K. Alam, T. Nuutinen, E. Hulkko, P. Karvinen, M. Kuittinen, J. J. Toppari, and E. M. Vartiainen, "Influence of Fano resonance on SERS enhancement in Fano-plasmonic oligomers," Opt. Express **27**(21), 30031–30043 (2019).
24. L. Stern, M. Grajower, and U. Levy, "Fano resonances and all-optical switching in a resonantly coupled plasmonic-atomic system," Nat. Commun. **5**(1), 4865 (2014).
25. N. Dabidian, I. Kholmanov, A. B. Khanikaev, K. Tatar, S. Trendafilov, S. H. Mousavi, C. Magnuson, R. S. Ruoff, and G. Shvets, "Electrical Switching of Infrared Light Using Graphene Integration with Plasmonic Fano Resonant Metasurfaces," ACS Photonics **2**(2), 216–227 (2015).
26. A. Karvounis, B. Gholipour, K. F. Macdonald, and N. I. Zheludev, "All-dielectric phase-change reconfigurable metasurface," Appl. Phys. Lett. **109**(5), 051103 (2016).
27. J. Jiang, R. Fang, J. Han, F. Wu, and Y. Yang, "Optical switching of terahertz wave based on asymmetric metamaterial structures," Ferroelectrics **568**(1), 79–84 (2020).
28. C. Wu, N. Arju, G. Kelp, J. A. Fan, J. Dominguez, E. Gonzales, E. Tutuc, I. Brener, and G. Shvets, "Spectrally selective chiral silicon metasurfaces based on infrared Fano resonances," Nat. Commun. **5**(1), 3892 (2014).
29. X. Tian, Z. Liu, H. Lin, B. Jia, Z.-Y. Li, and J. Li, "Five-fold plasmonic Fano resonances with giant bisignate circular dichroism," Nanoscale **10**(35), 16630–16637 (2018).
30. T. Cao, L. Mao, Y. Qiu, L. Lu, A. Banas, K. Banas, R. E. Simpson, and H.-C. Chui, "Fano Resonance in Asymmetric Plasmonic Nanostructure: Separation of Sub-10 nm Enantiomers," Adv. Opt. Mater. **7**(3), 1801172 (2019).
31. Y. Cui, J. Zhou, V. A. Tamma, and W. Park, "Dynamic Tuning and Symmetry Lowering of Fano Resonance in Plasmonic Nanostructure," ACS Nano **6**(3), 2385–2393 (2012).
32. N. K. Emani, T.-F. Chung, A. V. Kildishev, V. M. Shalaev, Y. P. Chen, and A. Boltasseva, "Electrical Modulation of Fano Resonance in Plasmonic Nanostructures Using Graphene," Nano Lett. **14**(1), 78–82 (2014).
33. Y. Vardi, E. Cohen-Hoshen, G. Shalem, and I. Bar-Joseph, "Fano Resonance in an Electrically Driven Plasmonic Device," Nano Lett. **16**(1), 748–752 (2016).
34. N. Verellen, Y. Sonnefraud, H. Sobhani, F. Hao, V. V. Moshchalkov, P. V. Dorpe, P. Nordlander, and S. A. Maier, "Fano Resonances in Individual Coherent Plasmonic Nanocavities," Nano Lett. **9**(4), 1663–1667 (2009).
35. S. Panaro, F. De Angelis, and A. Toma, "Dark and bright mode hybridization: From electric to magnetic Fano resonances," Optics and Lasers in Engineering **76**, 64–69 (2016).
36. F. Shafiei, F. Monticone, K. Q. Le, X.-X. Liu, T. Hartsfield, A. Alù, and X. Li, "A subwavelength plasmonic metamolecule exhibiting magnetic-based optical Fano resonance," Nat. Nanotechnol. **8**(2), 95–99 (2013).
37. A. Nazir, S. Panaro, R. Proietti Zaccaria, C. Liberale, F. De Angelis, and A. Toma, "Fano Coil-Type Resonance for Magnetic Hot-Spot Generation," Nano Lett. **14**(6), 3166–3171 (2014).

Optics EXPRESS

38. L. S. Slaughter, Y. Wu, B. A. Willingham, P. Nordlander, and S. Link, "Effects of Symmetry Breaking and Conductive Contact on the Plasmon Coupling in Gold Nanorod Dimers," ACS Nano **4**(8), 4657–4666 (2010).
39. I. Al-Naib, E. Hebestreit, C. Rockstuhl, F. Lederer, D. Christodoulides, T. Ozaki, and R. Morandotti, "Conductive Coupling of Split Ring Resonators: A Path to THz Metamaterials with Ultrasharp Resonances," Phys. Rev. Lett. **112**(18), 183903 (2014).
40. T. G. Habteyes, S. Dhuey, S. Cabrini, P. J. Schuck, and S. R. Leone, "Theta-Shaped Plasmonic Nanostructures: Bringing "Dark" Multipole Plasmon Resonances into Action via Conductive Coupling," Nano Lett. **11**(4), 1819–1825 (2011).
41. Z. Liu, Z. Liu, J. Li, W. Li, J. Li, C. Gu, and Z.-Y. Li, "3D conductive coupling for efficient generation of prominent Fano resonances in metamaterials," Sci. Rep. **6**(1), 27817 (2016).
42. Z. Liu, J. Li, Z. Liu, W. Li, J. Li, C. Gu, and Z.-Y. Li, "Fano resonance Rabi splitting of surface plasmons," Sci. Rep. **7**(1), 8010 (2017).
43. J. C. Prangsma, J. Kern, A. G. Knapp, S. Grossmann, M. Emmerling, M. Kamp, and B. Hecht, "Electrically connected resonant optical antennas," Nano Lett. **12**(8), 3915–3919 (2012).
44. J. Kern, R. Kullock, J. Prangsma, M. Emmerling, M. Kamp, and B. Hecht, "Electrically driven optical antennas," Nat. Photonics **9**(9), 582–586 (2015).
45. W. Zhang, L. Huang, C. Santschi, and O. J. Martin, "Trapping and sensing 10 nm metal nanoparticles using plasmonic dipole antennas," Nano Lett. **10**(3), 1006–1011 (2010).
46. L.-J. Black, Y. Wang, C. H. de Groot, A. Arbouet, and O. L. Muskens, "Optimal Polarization Conversion in Coupled Dimer Plasmonic Nanoantennas for Metasurfaces," ACS Nano **8**(6), 6390–6399 (2014).
47. P. B. Johnson and R. W. Christy, "Optical Constants of the Noble Metals," Phys. Rev. B **6**(12), 4370–4379 (1972).
48. H. Chen, T. Ming, S. Zhang, Z. Jin, B. Yang, and J. Wang, "Effect of the Dielectric Properties of Substrates on the Scattering Patterns of Gold Nanorods," ACS Nano **5**(6), 4865–4877 (2011).
49. H. Chen, L. Shao, T. Ming, K. Choi Woo, Y. Cho Man, J. Wang, and H.-Q. Lin, "Observation of the Fano Resonance in Gold Nanorods Supported on High-Dielectric-Constant Substrates," ACS Nano **5**(8), 6754–6763 (2011).
50. A. M. Kern and O. J. F. Martin, "Surface integral formulation for 3D simulations of plasmonic and high permittivity nanostructures," J. Opt. Soc. Am. A **26**(4), 732–740 (2009).
51. Y. Ekinci, A. Christ, M. Agio, O. J. F. Martin, H. H. Solak, and J. F. Löffler, "Electric and magnetic resonances in arrays of coupled gold nanoparticle in-tandem pairs," Opt. Express **16**(17), 13287–13295 (2008).
52. C. Yan, K.-Y. Yang, and O. J. F. Martin, "Fano-resonance-assisted metasurface for color routing," Light: Sci. Appl. **6**(7), e17017 (2017).
53. A. Farhang and O. J. F. Martin, "Plasmon delocalization onset in finite sized nanostructures," Opt. Express **19**(12), 11387–11396 (2011).
54. B. Gallinet and O. J. F. Martin, "Ab initio theory of Fano resonances in plasmonic nanostructures and metamaterials," Phys. Rev. B **83**(23), 235427 (2011).
55. B. Gallinet, T. Siegfried, H. Sigg, P. Nordlander, and O. J. F. Martin, "Plasmonic Radiance: Probing Structure at the Ångström Scale with Visible Light," Nano Lett. **13**(2), 497–503 (2013).
56. R. H. Harrington, *Field computation by the moment methods* (IEEE Series on Electromagnetic Waves, 1993).
57. C. L. Garrido Alzar, M. A. G. Martinez, and P. Nussenzveig, "Classical analog of electromagnetically induced transparency," Am. J. Phys. **70**(1), 37–41 (2002).
58. S. Satpathy, A. Roy, and A. Mohapatra, "Fano interference in classical oscillators," Eur. J. Phys. **33**(4), 863–871 (2012).
59. B. Gallinet, A. Lovera, T. Siegfried, H. Sigg, and O. J. F. Martin, "Fano resonant plasmonic systems: Functioning principles and applications," in *AIP Conference Procedings*, vol. 1475 (2012), pp. 18–20.
60. B. Abasahl, C. Santschi, and O. J. F. Martin, "Quantitative Extraction of Equivalent Lumped Circuit Elements for Complex Plasmonic Nanostructures," ACS Photonics **1**(5), 403–407 (2014).